Transient Kinetics of O2 Evolution in Photocatalytic Water-Splitting Reaction

Kosaka, Takumu ; Teduka, Yuya ; Ogura, Takuya ; Zhou, Yuanshu ; Hisatomi, Takashi ; Nishiyama, Hiroshi ; Domen, Kazunari ; Takahashi,…

(Citation)
ACS Catalysis,10(22):13159-13164

(Issue Date)
2020-11-20

(Resource Type)
journal article

(Version)
Version of Record

ACS Catalysis

pubs.acs.org/acscatalysis Letter

Transient Kinetics of O_2 Evolution in Photocatalytic Water-Splitting Reaction

Takumu Kosaka, Yuya Teduka, Takuya Ogura, Yuanshu Zhou, Takashi Hisatomi, Hiroshi Nishiyama, Kazunari Domen, Yasufumi Takahashi, and Hiroshi Onishi*

Cite This: *ACS Catal.* 2020, 10, 13159–13164 Read Online

ACCESS | Metrics & More | Article Recommendations | Supporting Information

ABSTRACT: Water splitting to produce H_2 and O_2 is a fundamental reaction for artificial photosynthesis on semiconductor photocatalysts. The mechanism of the multistepped reaction, especially four-electron oxidation to O_2, has not yet been understood. Although some intermediate states have been detected in transient spectroscopy, O_2 evolution kinetics remain unknown at the end of consecutive reaction steps. We apply operando O_2 detection with a microelectrode to determine the absolute evolution rate on a highly efficient $SrTiO_3$ photocatalyst film casted on a glass plate. The evolution rate was determined with a time resolution of 0.1 s, which was improved by 1000 times compared with that in widely used gas-chromatographic detection. The observed rate did not respond instantaneously to excitation light irradiation. When light was turned on, the photocatalyst film was inactive for evolution and light-activated in seconds. It was proposed that the first absorbed photons were consumed to fill trap states on $SrTiO_3$ surface and then the latter photons drove steady O_2 evolution. When excitation light stopped, the O_2 evolution rate exponentially decayed in seconds. The microelectrode method demonstrated herein will be useful for understanding many other reaction kinetics at liquid–solid interfaces.

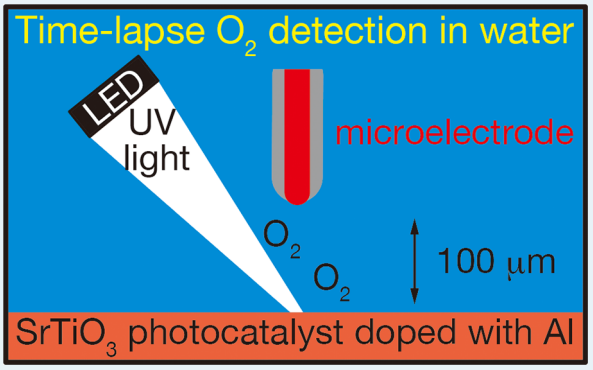

KEYWORDS: *artificial photosynthesis, mechanism, microelectrode, reaction rate, strontium titanate*

The oxidation of water to O_2 is a longstanding problem in the field of sustainable energy.[1−4] Understanding the oxidation kinetics is of fundamental interest for artificial photosynthesis over semiconductor photocatalysts. This is because the electrons involved in the water reduction to hydrogen or CO_2 reduction to organic compounds must be provided by water oxidation when applied at a practical scale.[5]

Light irradiation initiates a cycle of elementary reactions to split water and produce O_2 and H_2. Oxygen evolution requires four-electron oxidation of water, while hydrogen is produced with two electrons. The rate-limiting step in a steady state may shift from one to another according to choice of photocatalyst semiconductor, cocatalyst, pH of water, and so on. The foremost intermediate states, electrons and holes excited in the semiconductor, can be quantified with a time resolution of nanoseconds to milliseconds by detecting visible[6,7] or infrared[8,9] light absorption, microwave reflection,[10] and electron spin resonance.[11] Infrared absorption[12−14] and electron spin resonance[15] can also reveal the structure of short-lived chemical species in the middle of the cycle. The transient kinetics of the final product evolution are unknown, although they are necessary to obtain a complete picture of the cycled reactions. O_2 detection with a comparable time resolution remains a challenge to experimental researchers.

The steady-state rate of O_2 evolution is determined using gas chromatography and is reported in units of mol per hour. By improving the gas sampling speed, the time resolution was improved to minutes,[16] which was sufficient to observe transient hole consumption for oxidizing Ni@NiO_x cocatalyst nanoparticles loaded on a $SrTiO_3$ photocatalyst. The time resolution in chromatographic detection is limited by the physical distance between the reactor and detector.

Electrochemical detection provides a method of introducing a detector into the reactor. Scanning electrochemical microscopy (SECM)[17] is particularly effective for shortening the diffusion length to the detector. A micrometer-sized electrode is moved close to a solid object in an electrolyte solution. Chemical compounds are released on the object, diffused across the electrode–object gap, and converted to a current on the electrode. Localized O_2 evolution has been detected and even mapped on patterned Fe_2O_3,[18] $SrTiO_3$,[19]

Received: September 20, 2020
Revised: October 27, 2020
Published: October 29, 2020

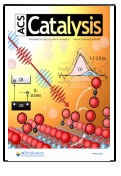

https://dx.doi.org/10.1021/acscatal.0c04115
ACS Catal. 2020, 10, 13159–13164

and TiO_2[20−22] as well as H_2O_2 evolution on Fe_2O_3.[23] In the present study, we exploited the quick current response allowed by shortened diffusion lengths for the quantitative analysis of the O_2 evolution rate in a time resolution of 0.1 s.

A $SrTiO_3$ photocatalyst doped with Al cations was prepared in $SrCl_2$ flux at 1423 K. The molar ratio of $SrTiO_3$ and Al_2O_3 was 100:2 in the starting material. A $RhCrO_x$ cocatalyst (Rh 0.1 wt % and Cr 0.1 wt %) was loaded on the doped photocatalyst particles by impregnation from an aqueous solution of Na_3RhCl_6 and $Cr(NO_3)_3$. A CoO_y cocatalyst (Co 0.1 wt %) was additionally loaded thorough photodeposition in an aqueous solution of $CoCl_2$. The cocatalyst-loaded photocatalyst was suspended in water with nanometer-sized SiO_2 particles (1:2 in weight ratio), dropped on a frosted glass plate, and dried at 323 K to form a photocatalyst film (thickness: 10−20 μm) that is stable in aqueous solutions. The film was casted on the glass plate and electrically isolated in the electrolyte solution. Hence, the water-splitting reaction was photocatalytically driven on the film free from external bias voltage. Photocatalyst films prepared in a similar manner are placed in a panel reactor and being tested for large-scale water splitting under natural sunlight. Details of photocatalyst preparation, drop casting, and testing under sunlight are available in ref 24.

The experimental setup, which was based on our earlier study,[25] is briefly described herein, and details are available in the Supporting Information. A millimeter-sized piece of the photocatalyst-casted plate was immersed in a KCl aqueous solution (pH = 7) at room temperature, and its front surface was side lit with ultraviolet (UV) light (center wavelength: 280 nm) with a 3 W m^{-2} intensity (4×10^{18} photons m^{-2} s^{-1}) passing through the solution surface. The light intensity was reduced to produce H_2 and O_2 dissolved in the solution without forming bubbles on the film. Platinum wire with a 10-μm radius was wrapped in glass to expose a metal section at one end as the working electrode for O_2 detection (Figures S1, S2). The electrode was immersed in the solution perpendicular to the photocatalyst film with controlled electrode−film distances in a range of 100−200 μm with a precision of 0.1 μm (Figure S4). Molecular oxygen that was photocatalytically produced on the film and released into the solution was electrochemically detected on the electrode biased at −0.5 V relative to a Ag wire as the counter electrode. Four-electron reduction, $O_2 + 2H_2O + 4e^- \rightarrow 4OH^-$ and/or $O_2 + 4H^+ + 4e^- \rightarrow H_2O$,[26] generated an electrode current on the order of nanoamps that was proportional to O_2 concentration (Figure S3). The standard deviation of the electrode current averaged for 0.1 s was 3 pA, which corresponded to an O_2 concentration deviation of 0.1 μM. The whole setup was installed in a glovebox filled with N_2 gas to remove O_2 that was dissolved in the solution.

Figure 1A presents the electrochemical current response ΔI induced by the UV light irradiation at an electrode−film distance d = 100 μm. The negative sign of the current response represents electrons transferred from the electrode to the solution. Residual O_2 in the solution produced a background current of less than −0.04 nA, which was subtracted to deduce the irradiation-induced current response. When UV light was turned on at t = 0, ΔI continuously increased and then gradually decreased back to zero when the light was turned off at 101.5 s. Possible contribution of the UV-irradiated electrode or KCl electrolyte to the photoinduced current response was examined and excluded (Figures S7 and S8).

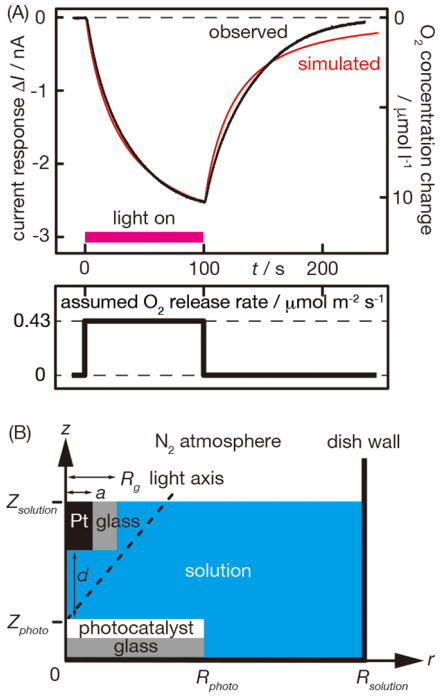

Figure 1. Electrochemical current response induced by UV light irradiation. A response curve (black) observed at an electrode−film distance d = 100 μm is shown in (A) with the simulated curve (red). The current response was converted to a local O_2 concentration change by using a current−concentration relation (Figure S3). The simulation space with cylindrical symmetry around the z-axis is illustrated in (B). Platinum electrode section radius a: 10 μm; glass wrap outer radius R_g: 20 μm; photocatalyst film radius R_{photo}: 670 μm; solution dish radius $R_{solution}$: 13 mm; solution thickness $Z_{solution}$: 10 mm; glass plate thickness Z_{photo}: 1 mm. The axis of excitation light was inclined by 50° from the solution surface in the plane involving z axis and an LED light source.

An increase or decrease in the observed current response did not necessarily correspond to the O_2 release rate on the film, because the local O_2 concentration monitored with the microelectrode was determined by balancing the O_2 release rate on the film and the O_2 diffusion rate to the bulk solution. A numerical simulation involving release and diffusion was required to determine the release rate on the film.

The simulation space defined in cylindrical coordinates, r and z, is illustrated in Figures 1B and S9. Oxygen diffusion driven by a concentration gradient is described by Fick's law:

$$\frac{\partial C}{\partial t} = D\left(\frac{\partial^2 C}{\partial r^2} + \frac{1}{r}\frac{\partial C}{\partial r} + \frac{\partial^2 C}{\partial z^2}\right)$$

with concentration C and diffusion coefficient $D = 2.5 \times 10^{-5}$ cm^2 s^{-1} at 298 K.[27] The details of the finite-element scheme for integrating the equation using COMSOL Multiphysics to predict the current response are described in the Supporting Information. The instantaneous O_2 release at a constant rate of 0.43 μmol m^{-2} s^{-1} was assumed during the light irradiation and fitted to the experimentally observed current response, as shown in Figure 1A. Though the release rate was constant on the film, the current response gradually increased as the O_2-rich portion spatially expanded in the solution (Figure S10). Two more response curves were observed by changing d to 150 and 200 μm (Figure S5), and the curves were fitted to validate the simulation scheme. An additional measurement

https://dx.doi.org/10.1021/acscatal.0c04115
ACS Catal. 2020, 10, 13159−13164

was conducted with d = 120 μm using a different electrode to confirm the reproducibility of the electrochemical current response (Figure S6).

Thermally induced convection, if any, should perturb O_2 diffusion driven by concentration gradient. However, the ΔI curve simulated in Fick's law fitted the observed response, as shown in Figure 1A. A possible reason for the limited contribution of thermal convection could be in thermal diffusivity in water (1.5×10^{-3} cm^2 s^{-1})[28] much larger than the O_2 diffusion constant (2.5×10^{-5} cm^2 s^{-1}). The large thermal diffusivity offers a small temperature gradient and thus the limited role of thermal convection in O_2 transport.

The apparent quantum yield in the O_2 evolution, which is defined as the number ratio of holes consumed in the four-electron oxidation to the number of incident photons, was estimated to be 24% on the basis of the fitted release rate and light intensity. Similarly prepared photocatalyst particles, which were not diluted with SiO_2, exhibited an apparent quantum yield of 55% with excitation light wavelengths of 340−360 nm when suspended in water.[24] A quantitative discrepancy by a factor of 2 remained between the yield on the film and that in the suspension. The uncertainty in the light intensity on the film and O_2 diffusion constant can be the reason for the discrepancy. Additional description about the uncertainties is available in section 1 of Supporting Information. Light scattering enhanced by SiO_2 nanoparticles may also have caused a lower light absorption probability on the film, since refractive index of SiO_2 (1.6 at 300 nm)[29] is slightly higher than the index of water (1.4 at 300 nm).[29]

The current response was further investigated in a time window of 0−10 s (Figure 2), since the characteristic time for diffusion across the electrode−film gap was d^2/D = 4 s. The assumption of an instantaneous O_2 release with no time delay, which was successfully applied in the window of 0−200 s (Figure 1), failed to fit the real response in the window of 0−10 s. ΔI increased slower than in the simulated curve, indicating that the rise time in the O_2 release rate was finite. The release rate was modeled as a step function that jumped from 0 to 0.43 μmol m^{-2} s^{-1} with a delay of 1 or 2 s in Figure 2A. The real response was close to the simulated curve that was delayed by 1 s at t = 0−5 s, and the other curve that was delayed by 2 s at t = 5−10 s.

The real response was not yet identical to the curves simulated with the delayed step functions. A release rate proportional to $1 - e^{-t/\tau}$ yielded the best fit with a time constant τ = 1.5 s, as shown in Figure 2B. The O_2 release rate gradually increased from zero to the steady number (0.43 μmol m^{-2} s^{-1}) in the best fit function. The authors interpret the function with a two-states model of the photocatalyst film. The film was uniformly inactive (no O_2 evolution even under light irradiation) at t = 0 and converted to an active state (0.43 μmol m^{-2} s^{-1} evolution under light irradiation) by photon absorption. It is additionally assumed that the first absorbed photon locally activated a small segment where the photon was absorbed. The second and latter photons absorbed at activated segments drove the steady O_2 evolution. The fraction of the inactive state x decreases with light irradiation time along $\frac{dx}{dt} = -kx$ since photons hit the film randomly in space. The constant k is given by the product of photon flux and segment area activated by one photon absorption. The fraction of the active state increases with $1 - e^{-t/\tau}$ on this assumption, and the reciprocal of k gives time constant τ. The interpretation

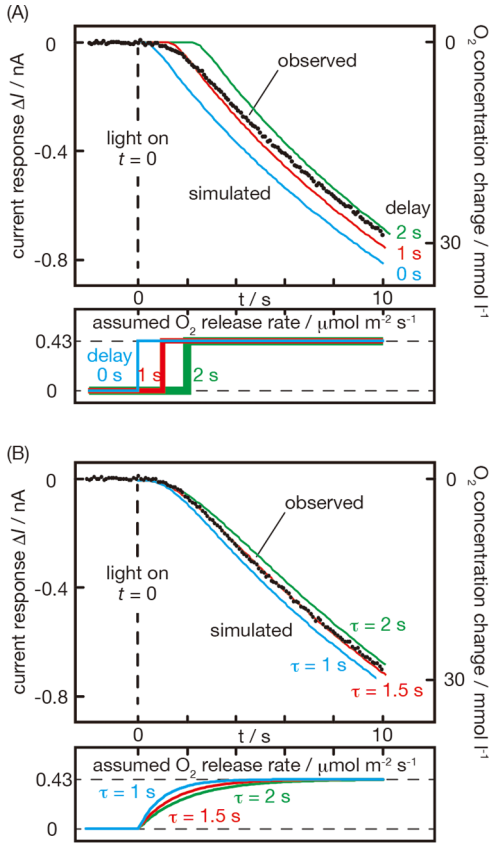

Figure 2. Initial current response induced by irradiation. The current response observed at d = 100 μm is shown with the simulated curves. The O_2 release rate was assumed to have the form of (A) a delayed step function with delays of 0 (blue curves), 1 (red curves), and 2 s (green curves). The curves in (B) were simulated with a release rate proportional to $1 - e^{-t/\tau}$, with τ values of 1 (blue curves), 1.5 (red curves), and 2 s (green curves).

proposed here predicts the gradual change of macroscopic evolution rate as a result of microscopic two-states conversion.

Consider further a possible mechanism of light activation. A limited number of electronic states in the bandgap, occupied or unoccupied, should be present in real photocatalysts. Bandgap-excited holes (electrons) are trapped in the occupied (unoccupied) states to reduce or even lose their potential for the water-splitting reaction, as was proposed for GaN:ZnO photocatalysts.[30] Excited electrons and holes first fill the trap states. The photocatalyst is then functional for water splitting. The area density of the trap states to be filled was estimated as 6×10^{18} m^{-2} on our film as the product of the photon flux and τ. The estimated trap-state density agreed with the surface unit cell density of crystalline $SrTiO_3$, with a value of 6.6×10^{18} m^{-2} on its (100) truncation.[31] This agreement allowed us to infer that the trap states were present on the $SrTiO_3$ surface in a one-trap-per-one-unit-cell fashion.

Finally, the current response observed with light irradiation stopped at t = 101.5 s was simulated. The O_2 release rate exponentially decayed with a fitted time constant δ of 2 s (Figure 3), whereas instantaneous suspension (δ = 0) failed to follow the real response. The exponential decay would have been induced by thermally activated desorption of the O_2 that was produced and adsorbed on the film. First-order desorption with an activation energy of 76 kJ mol^{-1} and a frequency factor of 1×10^{13} s^{-1} satisfied the observed time constant at room

https://dx.doi.org/10.1021/acscatal.0c04115
ACS Catal. 2020, 10, 13159−13164

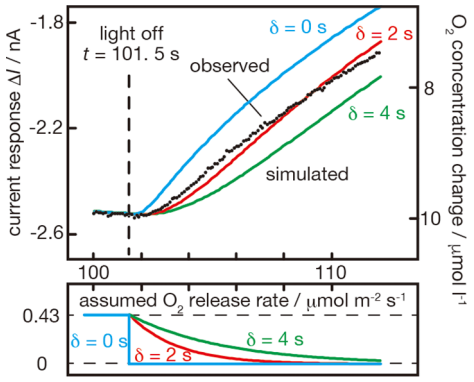

Figure 3. Current response observed at t = 100−112 s and simulated curves with O_2 release rates proportional to $e^{-(t-101.5s)/\delta}$. The decay time constant δ had values of 0 (blue curves), 2 (red curves), and 4 s (green curves).

temperature. Desorption of a chemically adsorbed species, possibly O_2 in a charged or neutral state, requires bond rupture between O_2 and the substrate. An activation energy in the order of 100 kJ mol^{-1} is natural for the bond rupture when thermally activated. The electronically excited states that enabled O_2 evolution decayed following the first-order kinetics provide another scheme of interpretation. Bandgap-excited states often decay slowly in semiconductors efficient for photocatalytic reactions.[8] $SrTiO_3$ particles doped with Na cations provides one example related to our photocatalyst film. A transient absorption study[32] found that excited electrons and holes detectable at delay times of 1 ms or longer when the particles were excited in a vacuum. Electron/hole decay kinetics in liquid water should be examined in a future study and related to light-off transient of O_2 evolution.

In the present study, we attempted to quantitatively determine the transient response of photocatalytic O_2 evolution in water. Microelectrochemical detection combined with the diffusion simulations provided the absolute evolution rate with a time resolution of 0.1 s on the $SrTiO_3$ photocatalyst film, which is being tested for large-scale water splitting under sunlight. The observed rate responded to excitation light irradiation with delay times in the order of seconds. Catalysis researchers including ourselves assumed photocatalytic conversion of materials instantaneously responding to light irradiation. The present study revealed a new physical insight beyond the assumption.

In addition, the method demonstrated herein will help us to understand many other reaction kinetics at liquid−solid interfaces. Thermal or photoinduced desorption coupled with mass spectroscopy has been a standard protocol to detect chemical species produced at vapor−solid interfaces in a time-resolved fashion.[33] For analyzing electrochemical reactions, differential electrochemical mass spectroscopy (DEMS)[34] has been developed. In DEMS, the working electrode is deposited on a porous, hydrophobic membrane. Volatile products formed on the electrode are sucked thorough the membrane into the ionizer of a mass spectrometer. Application to electrochemical O_2 evolution was conducted on Pt[35] and Ru[36] electrodes, while not yet applied to photocatalysts. DEMS limits itself in characterizing materials deposited on a membrane. The microelectrode method developed in the present study is applicable to any materials and even devices assembled for a practical application. One definite merit of DEMS is mass sensitivity in product detection that allows isotope labeling when necessary.

Volatile compounds released on the polymer membrane irradiated with UV light might be problematic in applying DEMS to photocatalysts. Different cell designs were successfully examined to separate the working electrode from the membrane.[37,38] On the other hand, additional time (1−2 s) is required to transfer species formed at the electrode to the membrane.[39] The time resolution in transient response should be limited by separating the membrane. Hence, the authors find our principle of shortening reactor-to-microelectrode distance is advantageous for observing transient response of photocatalytic reactions.

The microelectrode method is similar to voltammetry with a rotating ring-disk electrode[40] in shortening reactor−detector distance. Chemical species are produced on the disk electrode, transported in the centrifugal solution flow over the rotating electrode assembly, and detected on the ring electrode surrounding the disk. The rotating ring-disk setup provides a nice tool to determine steady-state rate of electrochemical reactions. However, it is not optimized for detecting transient response of photocatalytic reactions. The time resolution in product detection should be sensitive to electrode dimensions, especially the disk-to-ring gap distance. The authors are concerned about assembling a photocatalyst disk surrounded by a ring electrode with a controlled gap distance. Instead, they developed the scanning microelectrode method to control the electrode−object gap with a precision of 0.1 μm.

■ ASSOCIATED CONTENT

Supporting Information

The Supporting Information is available free of charge at https://pubs.acs.org/doi/10.1021/acscatal.0c04115.

Experimental and simulation details including Figures S1−S10 (PDF)

■ AUTHOR INFORMATION

Corresponding Author

Hiroshi Onishi − *Department of Chemistry, School of Science, Kobe University, Kobe 657-8501, Japan;* orcid.org/0000-0003-1873-9105; Email: oni@kobe-u.ac.jp

Authors

Takumu Kosaka − *Department of Chemistry, School of Science, Kobe University, Kobe 657-8501, Japan*

Yuya Teduka − *Department of Chemistry, School of Science, Kobe University, Kobe 657-8501, Japan*

Takuya Ogura − *Department of Chemistry, School of Science, Kobe University, Kobe 657-8501, Japan*

Yuanshu Zhou − *Nano Life Science Institute, Kanazawa University, Kanazawa 920-1192, Japan*

Takashi Hisatomi − *Interdisciplinary Cluster for Cutting Edge Research, Shinshu University, Nagano 380-8553, Japan;* orcid.org/0000-0002-5009-2383

Hiroshi Nishiyama − *Office of University Professors, The University of Tokyo, Tokyo 113-8656, Japan*

Kazunari Domen − *Interdisciplinary Cluster for Cutting Edge Research, Shinshu University, Nagano 380-8553, Japan; Office of University Professors, The University of Tokyo, Tokyo 113-8656, Japan;* orcid.org/0000-0001-7995-4832

Yasufumi Takahashi − *Nano Life Science Institute, Kanazawa University, Kanazawa 920-1192, Japan; Precursory Research*

https://dx.doi.org/10.1021/acscatal.0c04115
ACS Catal. 2020, 10, 13159−13164

for Embryonic Science and Technology, Japan Science and Technology Agency, Saitama 332-0012, Japan; orcid.org/0000-0003-2834-8300

Complete contact information is available at: https://pubs.acs.org/10.1021/acscatal.0c04115

Author Contributions

The manuscript was written through contributions of all authors.

Notes

The authors declare no competing financial interest.

■ ACKNOWLEDGMENTS

Yasuko Kuromiya, Yoshie Nagatuma, and Masaharu Yamaguchi are thanked for their technical assistance. This work was supported by JSPS KAKENHI, grant numbers JP16H02250 and JP19H00915. Y. T. acknowledges support from PRESTO (JPMJPR18T8) from the Japan Science and Technology Agency.

■ REFERENCES

(1) Fabbri, E.; Schmidt, T. J. Oxygen Evolution Reaction—The Enigma in Water Electrolysis. *ACS Catal.* **2018**, *8*, 9765−9774.
(2) Song, F.; Bai, L.; Moysiadou, A.; Lee, S.; Hu, C.; Liardet, L.; Hu, X. Transition Metal Oxides as Electrocatalysts for the Oxygen Evolution Reaction in Alkaline Solutions: An Application-inspired Renaissance. *J. Am. Chem. Soc.* **2018**, *140*, 7748−7759.
(3) Zhu, S.; Zhao, Y.; He, Y.; Wang, D. Selectivity of H_2O_2 and O_2 by Water Oxidation on Metal Oxide Surfaces. *J. Chem. Phys.* **2019**, *150*, No. 041712.
(4) Rossmeisl, J.; Qu, Z.-W.; Zhu, H.; Kroes, G.-J.; Nørskov. Electrolysis of Water on Oxide Surfaces. *J. Electroanal. Chem.* **2007**, *607*, 83−89.
(5) Inoue, H.; Shimada, T.; Kou, Y.; Nabetani, Y.; Masui, D.; Takagi, S.; Tachibana, H. The Water Oxidation Bottleneck in Artificial Photosynthesis: How can We Get Through It? An Alternative Route Involving a Two-electron Process. *ChemSusChem* **2011**, *4*, 173−179.
(6) Tang, J.; Durrant, J. R.; Klug, D. R. Mechanism of Photocatalytic Water Splitting in TiO_2. Reaction of Water with Photoholes, Importance of Charge Carrier Dynamics, and Evidence for Four-hole Chemistry. *J. Am. Chem. Soc.* **2008**, *130*, 13885−13891.
(7) Le Formal, F.; Pastor, E.; Tilley, S. D.; Mesa, C. A.; Pendlebury, R.; Grätzel, M.; Durrant, J. R. Rate Law Analysis of Water Oxidation on a Hematite Surface. *J. Am. Chem. Soc.* **2015**, *137*, 6629−6637.
(8) Yamakata, A.; Ishibashi, T.; Kato, H.; Kudo, A.; Onishi, H. Photodynamics of $NaTaO_3$ Catalysts for Efficient Water Splitting. *J. Phys. Chem. B* **2003**, *107*, 14383−14387.
(9) Jin, S.; Wang, W.; Wang, X.; Ju, M.; Shen, S.; Liang, W.; Zhao, Y.; Feng, Z.; Playford, H. Y.; Walton, R. I.; Li, C. Effect of Phase Junction Structure on the Photocatalytic Performance in Overall Water Splitting: Ga_2O_3 Photocatalyst as an Example. *J. Phys. Chem. C* **2015**, *119*, 18221−18228.
(10) Katoh, R.; Furube, A.; Yamanaka, K.; Morikawa, T. Charge Separation and Trapping in N-doped TiO_2 Photocatalysts: A Time-Resolved Microwave Conductivity Study. *J. Phys. Chem. Lett.* **2010**, *1*, 3261−3265.
(11) Rajh, T.; Poluektov, O.; Dubinski, A. A.; Wiederrecht, G.; Thurnauer, M. C.; Trifunac, A. D. Spin Polarization Mechanisms in Early Stages of Photoinduced Charge Separation in Surface-modified TiO_2 Nanoparticles. *Chem. Phys. Lett.* **2001**, *344*, 31−39.
(12) Zhang, M.; de Respinis, M.; Frei, H. Time-resolved Observations of Water Oxidation Intermediates on a Cobalt Oxide Nanoparticle Catalyst. *Nat. Chem.* **2014**, *6*, 362−367.
(13) Nakamura, R.; Nakato, Y. Primary Intermediates of Oxygen Photoevolution Reaction on TiO_2 (Rutile) Particles, Revealed by in situ FTIR Absorption and Photoluminescence Measurements. *J. Am. Chem. Soc.* **2004**, *126*, 1290−1298.
(14) Zandi, O.; Hamann, T. W. Determination of Photoelectrochemical Water Oxidation Intermediates on Haematite Electrode Surfaces Using operando Infrared Spectroscopy. *Nat. Chem.* **2016**, *8*, 778−783.
(15) Nosaka, Y.; Nosaka, A. Y. Generation and Detection of Reactive Oxygen Species in Photocatalysis. *Chem. Rev.* **2017**, *117*, 11302−11336.
(16) Han, K.; Kreuger, T.; Mei, B.; Mul, G. Transient Behavior of Ni@NiO_x Functionalized $SrTiO_3$ in Overall Water Splitting. *ACS Catal.* **2017**, *7*, 1610−1614.
(17) Bard, A. J.; Fan, F. R. F.; Kwak, J.; Lev, O. Scanning Electrochemical Microscopy. Introduction and Principles. *Anal. Chem.* **1989**, *61*, 132−138.
(18) Lee, J.; Ye, H.; Pan, S.; Bard, A. J. Screening of Photocatalysts by Scanning Electrochemical Microscopy. *Anal. Chem.* **2008**, *80*, 7445−7450.
(19) Plaza, M.; Huang, X.; Ko, J. Y. P.; Shen, M.; Simpson, B. H.; Rodríguez-López, J.; Ritzert, N. L.; Letchworth-Weaver, K.; Gunceler, D.; Schlom, D. G.; Arias, T. A.; Brock, J. D.; Abruña, H. D. Structure of the Photo-catalytically Active Surface of $SrTiO_3$. *J. Am. Chem. Soc.* **2016**, *138*, 7816−7819.
(20) Bae, J. H.; Nepomnyashchii, A. B.; Wang, X.; Potapenko, D. V.; Mirkin, M. V. Photo-scanning Electrochemical Microscopy on the Nanoscale with Through-tip Illumination. *Anal. Chem.* **2019**, *91*, 12601−12605.
(21) Zhou, X.; Gossage, Z. T.; Simpson, B. H.; Hui, J.; Barton, Z. J.; Rodríguez-López, J. Electrochemical Imaging of Photoanodic Water Oxidation Enhancements on TiO_2 Thin Films Modified by Subsurface Aluminum Nanodimers. *ACS Nano* **2016**, *10*, 9346−9352.
(22) Ikeda, K.; Sakai, H.; Baba, R.; Hashimoto, K.; Fujishima, A. Photocatalytic Reactions Involving Radical Chain Reactions Using Microelectrodes. *J. Phys. Chem. B* **1997**, *101*, 2617−2620.
(23) Krumov, M. R.; Simpson, B. H.; Counihan, M. J.; Rodríguez-López, J. In situ Quantification of Surface Intermediates and Correlation to Discharge Products on Hematite Photoanodes Using a Combined Scanning Electrochemical Microscopy Approach. *Anal. Chem.* **2018**, *90*, 3050−3057.
(24) Goto, Y.; Hisatomi, T.; Wang, Q.; Higashi, T.; Ishikiriyama, K.; Maeda, T.; Sakata, Y.; Okunaka, S.; Tokudome, H.; Katayama, M.; Akiyama, S.; Nishiyama, H.; Inoue, Y.; Takewaki, T.; Setoyama, T.; Minegishi, T.; Takata, T.; Yamada, T.; Domen, K. A Particulate Photocatalyst Water-splitting Panel for Large-scale Solar Hydrogen Generation. *Joule* **2018**, *2*, 509−520.
(25) Takahashi, Y.; Shevchuk, A. I.; Novak, P.; Babakinejad, B.; Macpherson, J.; Unwin, P. R.; Shiku, H.; Gorelik, J.; Klenerman, D.; Korchev, Y. E.; Matsue, T. Topographical and Electrochemical Nanoscale Imaging of Living Cells Using Voltage-switching Mode Scanning Electrochemical Microscopy. *Proc. Natl. Acad. Sci. U. S. A.* **2012**, *109*, 11540−11545.
(26) Yeager, E. Electrocatalysts for O_2 reduction. *Electrochim. Acta* **1984**, *29*, 1527−1537.
(27) *Handbook of Chemistry: Pure Chemistry*; 4th ed.; Chemical Society of Japan, Ed.; Maruzen: Tokyo, 1993; pp II−63.
(28) Thermal diffusivity was calculated with thermal conductivity (0.61 $W\ m^{-1}\ K^{-1}$ at 298 K) found in *CRC Handbook of Chemistry and Physics*; 92nd ed.; Haynes, W. M., Lide, D. R., Eds.; CRC Press: Boca Raton, 2011; pp 6−242.
(29) *CRC Handbook of Chemistry and Physics*; 92nd ed.; Haynes, W. M., Lide, D. R., Eds.; CRC Press: Boca Raton, 2011; pp 10-242−10-244.
(30) Godin, R.; Hisatomi, T.; Domen, K.; Durrant, J. R. Understanding the Visible-light Photocatalytic Activity of GaN:ZnO Solid Solution: The Role of $Rh_{2-y}Cr_yO_3$ Cocatalyst and Charge Carrier Lifetimes over Tens of Seconds. *Chem. Sci.* **2018**, *9*, 7546−7555.
(31) The surface unit cell density was calculated with the cubic unit cell length (0.390 nm) reported in Abramov, Y. A.; Tsirelson, V. G.;

Zavodnik, V. E.; Ivanov, S. A.; Brown, I. D. The Chemical Bond and Atomic Displacements in $SrTiO_3$ from X-ray Diffraction Analysis. *Acta Crystallogr., Sect. B: Struct. Sci.* **1995**, *51*, 942−951.
(32) Kato, K.; Jiang, J.; Sakata, Y.; Yamakata, A. Effect of Na-doping on Electron Decay Kinetics in $SrTiO_3$ Photocatalyst. *ChemCatChem* **2019**, *11*, 6349−6354.
(33) Engel, T.; Ertl, G. Surface Residence Times and Reaction Mechanism in the Catalytic Oxidation of CO on Pd(111). *Chem. Phys. Lett.* **1978**, *54*, 95−98.
(34) Wolter, O.; Heitbaum, J. Differential Electrochemical Mass Spectroscopy (DEMS) − A New Method for the Study of Electrode Processes. *Ber. Bunsenges. Phys. Chem.* **1984**, *88*, 2−6.
(35) Willsau, J.; Wolter, O.; Heitbaum, J. Does the Oxide Layer Take Part in the Oxygen Evolution Reaction on Platinum? A DEMS Study. *J. Electroanal. Chem. Interfacial Electrochem.* **1985**, *195*, 299−306.
(36) Wohlfahrt-Mehrens, M.; Heitbaum, J. Oxygen Evolution on Ru and RuO_2 Electrodes Studied Using Isotope Labelling and On-line Mass Spectrometry. *J. Electroanal. Chem. Interfacial Electrochem.* **1987**, *237*, 251−260.
(37) Baltruschat, H. Differential Electrochemical Mass Spectroscopy. *J. Am. Soc. Mass Spectrom.* **2004**, *15*, 1693−1706.
(38) *Design, Construction and Research Application of a Differential Electrochemical Mass Spectrometer (DEMS)*; Ashton, S. J.; Springer: Heidelberg, 2012; Chapter 2.
(39) Jusys, J.; Behm, R. J. Methanol Oxidation on a Carbon-Supported Pt Fuel Cell Catalyst − A Kinetic and Mechanistic Study by Differential Electrochemical Mass Spectrometry. *J. Phys. Chem. B* **2001**, *105*, 10874−10883.
(40) Albery, W. J.; Hitchman, M. L. *Ring-Disc Electrodes*; Oxford University Press: Oxford, 1971.

https://dx.doi.org/10.1021/acscatal.0c04115
ACS Catal. 2020, 10, 13159−13164